Korean J. Chem. Eng., 35(10), 2127-2132 (2018)
DOI: 10.1007/s11814-018-0121-x

pISSN: 0256-1115
eISSN: 1975-7220

Photo-synthesized copper phenylacetylide nanobelts with preferential photocatalytic active facet exposure

Xinglong Xie[‡], Yu Qiu[‡], Sen Zhao, Hai-Ying Jiang[†], and Jinjun Lu

Key Lab of Synthetic and Natural Functional Molecule Chemistry of Ministry of Education, College of Chemistry & Materials Science, Northwest University, Xi'an 710127, P. R. China
(*Received 29 March 2018 • accepted 18 July 2018*)

Abstract−We recently reported that PhC_2Cu nanobelt exhibits excellent photocatalytic degradation of organic pollutants and activation of molecular O_2. However, there has been no further research about the relationship between its crystal structure and photocatalytic activity. Herein, a new safe and energy-save method, photo-synthesis, to prepare PhC_2Cu nanobelts with preferential active exposure facet was developed. It was used to study the relationship between its crystal structure and photocatalytic activity, compared to the PhC_2Cu nanobelts prepared by thermal-synthesis method. The prepared samples were characterized by X-ray powder diffractometer (XRD), field-emission scanning electron microscopy (FE-SEM), ultraviolet-visible (UV-vis) absorbance spectra and diffuse reflectance spectra (UV-vis Abs and DRS), N_2 adsorption-desorption isotherms, FT-IR and Raman spectra. The degradation of MB experiments under visible light irradiation shows that the photocatalytic activity of PhC_2Cu prepared by photo-synthesis method is much higher than that by traditional thermal-synthesis method. Moreover, the photocatalytic mechanism of PhC_2Cu nanobelts was further studied by the photocatalytic generation of $O_2^{-\bullet}$ and •OH.

Keywords: Photocatalyst, PhC_2Cu Nanobelts, Preferential Facet Exposure, Preparation Method

INTRODUCTION

The development of visible-light-harvesting materials based on earth-abundant elements is essential for the sunlight-driven elimination of environmental pollutants [1]. The photocatalytic activity of such materials originates from the photoinduced electron or energy transfer, activating substrates or other reagents (e.g., molecular oxygen). Conjugated organic polymers (COPs) [2], metal-organic frameworks (MOFs) [3-10] and metal-organic coordination polymers (MOCPs) [11-14] are emerging new members of the earth-abundant-element-based class of materials. They possess manifold excited states [e.g., metal-to-ligand charge transfer (MLCT), ligand-to-metal charge transfer (LMCT), ligand-to-ligand charge transfer (LLCT), and charge-separated (CS) excited states] with tunable energetics (through modification of unit chemical structures or through non-covalent intermolecular interaction) [3-6,15-17]. In general, the photoinduced events are described as band-gap excitations that generate conduction-band electrons and valence-band holes. The self-assembling property of such materials enables simple heterogenization, which is highly advantageous for separation and recycling of these materials relative to their homogeneous analogues. Moreover, the long-range-ordered structures in MOFs and MOCPs contain meso/micropores that may benefit the substrate-surface interaction [7-9,14]. Several heterogeneous systems based on MOCPs (e.g., Ru, Zn, Ag and Cu^{II}) have been developed for catalytic selective oxidation and organic pollutants degradation. However, the relativities for these systems are still limited to organic dye substrates and hazardous oxidants/solvents (*tert*-butyl peroxo or H_2O_2) are also often required [11-14]. In our exploration of heterogeneous visible-light photocatalysts, we consider the potential catalytic activity in different reaction pathways, e.g., oxidative degradation by molecular oxygen activation (via reactive oxygen species), as well as the reductive detoxification of organic halides by dissociative electron transfer.

Naturally, earth abundant materials with visible light activity have always been desired in photoinduced redox chemistry for organic transformation and elimination of environmental hazard compounds. Copper is such a routinely encountered element in our daily life and may be unexciting at the first glance. Actually, it continuously plays an active role in science for its essential, life-saving biology, because of its diverse chemical properties in the following three chemical processes: Lewis acid catalysis, single-electron-transfer processes and two-electron-transfer reactions; this suggests it as an efficient catalyst in a large number of reactions [18]. However, Cu-based semiconductors (i.e., CuO and Cu_2O) did not play very well in photocatalysis field; this unfavorable situation may be resulting from the improper band structure of CuO [19] and chemical instability of Cu_2O [20]. More recently, we first applied copper-phenylacetylide (PhC_2Cu) coordiantion polymer in the degradations of organic pollutants and activation of molecular oxygen under visible light irradiations, which exhibits excellent photocatalytic activity [21]. The good activity originates from its suitable band gap, favorable structure for electron/hole separation, and strong reductivity of conduction band electrons. The results show that PhC_2Cu nanobelt is a prospective visible-light-driven photocatalyst.

However, the research about PhC_2Cu coordination polymer in

[†]To whom correspondence should be addressed.
E-mail: jianghy@nwu.edu.cn
[‡]X. X and Y. Q contributed equally.

photocatalytic activity is very limited. It is universally known that different preparation method can result in different physical and chemical properties [22,23], so the photocatalytic activity is also different for PhC_2Cu nanobelt. Moreover, the bumping often occurs during the traditional thermal-synthesis method process of PhC_2Cu, which is dangerous and is not suitable for practical applications. In this work, we applied photosynthesis method to prepare PhC_2Cu nanobelt with different crystal facet to that prepared by thermal method, which shows significantly improved photocatalytic activity. Moreover, photosynthesis method was carried out at room temperature, which is safe and energy-saving. The prepared PhC_2Cu nanobelt prepared by photo and thermal synthesis method was mainly characterized by X-ray diffractometer (XRD), field-emission electroscope (FE-SEM), UV-vis diffuse reflectance spectroscopy (UV-vis DRS), surface analyzer, FT-IR and Raman spectra. The photocatalytic activities were measured by the degradation of methylene blue (MB) in aqueous solutions. Furthermore, the generation of $O_2^{-\bullet}$ and •OH, the products of molecular oxygen activation, were also tested by the nitro blue tetrazolium (NBT) and coumarin (CA) method.

EXPERIMENTAL

1. Preparation

365 mg $CuCl_2 \cdot 2H_2O$ (0.05 M) was dissolved in 40 mL CH_3OH, forming a blue transparent solution. The blue precipitate appeared when 1,120 μL Et_3N (0.2 M) was added in the blue transparent solution. With further addition of 440 μL phenylacetylene (0.1 M), the blue precipitate became green [21]. The acquired green suspension was treated via two different methods, thermal and photo. Thermal-synthesis: the suspension was heated to 65 °C and kept for about 10 minutes, until the precipitate turned to light yellow. Photo-synthesis: the suspension was irradiated by visible light with the wavelength of 420 nm<λ<800 nm (300 W Xe-arc lamp, PLS-SXE300) for about 30 minutes, until the suspension turned to light yellow. The obtained light-yellow precipitate was separated by centrifugation and washed with deionized water and ethanol for several times. After that, the as-prepared precipitate was dried at 60 °C overnight, and ground in a quartzose mortar. The light-yellow powder was PhC_2Cu and was marked as CP@H (thermal-synthesized PhC_2Cu) and CP@P (photo-synthesized PhC_2Cu), respectively.

2. Characterization

The crystal structures were characterized by a Bruker D8 advance X-ray powder diffractometer (XRD). The morphology was observed by field-emission scanning electron microscopy (FE-SEM, Hitachi, S-4800). Ultraviolet-visible (UV-vis) diffuse reflectance spectra (DRS) were recorded on an UV-vis spectrophotometer (Lambda40p). The N_2 adsorption-desorption isotherms were measured by a surface analyzer (Tri Star-3010, Micromeritics, USA), and the specific areas were analyzed by the Brunauer-Emmett-Teller (BET) method. The IR transmission spectrum was obtained with a Fourier transform-infrared (FT-IR) spectrophotometer (EQUINOX-55, Bruker). Raman spectrum was obtained with a Fourier transform-raman spectrophotometer (Thermo, DXR2).

3. Activity Evaluation

The degradation of Methylene Blue (MB) was carried out to evaluate the photocatalytic activity of the prepared PhC_2Cu samples. A 300 W Xe arc lamp (PLS-SXE300/300UV) equipped with a wavelength cutoff filter (420 nm<λ<800 nm) was used as the light source to trigger the photocatalytic degradation of MB over CP@H and CP@P samples. 25 mg photocatalysts were dispersed in 50 mL of MB aqueous solution at a concentration of 2.6×10^{-5} M, and the suspension was continuously stirred in the dark for 1 h to establish equilibrium between the catalyst surface and MB molecular. The suspension was kept at room temperature by circulating water bath. During the irradiation, 3 mL of the suspension was sampled at 10 minute intervals, the catalyst and the MB solution were separated by centrifugation. The concentration changes of MB solutions were monitored by measuring the absorbance at λ=664 nm with a UV-vis spectrophotometer (SP-756). The degradation efficiency of MB at each time interval was calculated by A/A_0, where A and A_0 stand for the absorbance at a certain time and the initialized concentration of MB solutions.

In addition, to study the effects of different reactive oxygen species, MB was also degraded in the presence of NBT and tert-butyl alcohol (TBA), whereas NBT and TBA were the captor of $O_2^{-\bullet}$ and •OH, respectively.

4. The Measurements of $O_2^{-\bullet}$ and •OH

The photocatalytic generation of $O_2^{-\bullet}$ by CP@H and CP@P was determined by the degradation of NBT, which was monitored by the absorbance change at the wavelength of 259 nm [24,25]. The mole ratio of generated $O_2^{-\bullet}$ and degraded NBT was 4 : 1 according to the following equation (Eq. (1)). Specifically, 20 mg photocatalyst was suspended in 40 mL NBT aqueous solution with a concentration of 2.0×10^{-5} M. The light source was a Xe-arc lamp (PLS-SXE300) equipped with a wavelength cutoff filter of 420 nm< λ<800 nm, and the suspension was kept at room temperature by circulating water bath. Before irradiation, the suspension was continuously stirred in the dark for 1 h. At the given time interval of 10 min, 3 mL of reaction suspension was sampled. The photocatalyst and the generated purple precipitate were separated by centrifugation, and then the absorbance of supernatant was recorded on a UV-vis spectrophotometer (Thermo, DXR2).

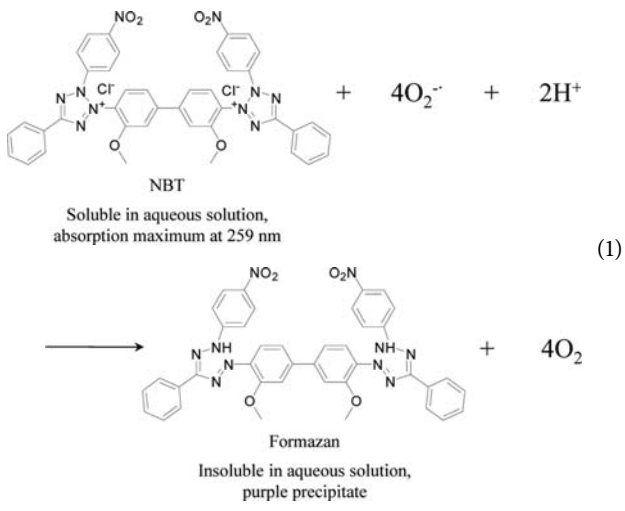

(1)

The photocatalytic generation of •OH over CP@H and CP@P was measured by fluorescence using coumarin (CA) as a chemical

trap (Eq. (2)) [26]. Typically, 25 mg photocatalyst was dissolved in 50 mL aqueous solution containing 1 mM coumarin. After being stirred in the dark for 30 minutes, the mixture was irradiated with visible light (420 nm<λ<800 nm). At the given time interval of 10 min, 2.5 mL of reaction suspension was sampled. If the •OH was formed, it would react with coumarin to form highly fluorescent 7-hydroxy-coumarin. As a result, the concentration of •OH was monitored by real time detection of fluorescence intensity on a spectrofluorometer (F-4500, Japan).

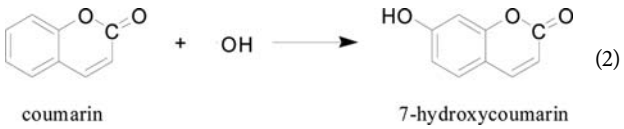

(2)

coumarin 7-hydroxycoumarin

RESULTS AND DISCUSSION

The as-prepared samples show similar diffraction patterns identified by XRD in Fig. 1, which is accordance with the standard crystallographic data reported in the Cambridge Crystallographic Data Centre (CCDC-242490), indicating that the two samples are all PhC_2Cu crystals [27]. Significantly, obvious difference in the intensity ratios for various peaks were observed. Specifically, the ratios of (001)/(100), (010)/(100) and (110)/(100) are, respectively, 0.173, 0.066 and 0.168 for CP@H sample, while they are 0.647, 0.394 and 0.459 for CP@P sample. In addition, the d-spacings of

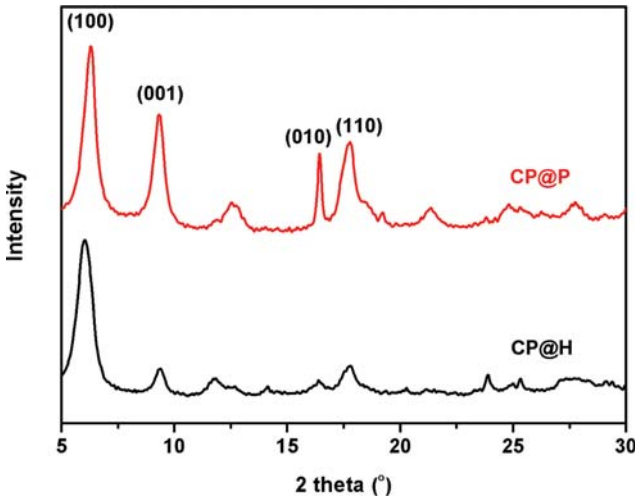

Fig. 1. XRD patterns of CP@H and CP@P solids.

(100) facet are also different for the two samples, which are 1.46 nm and 1.40 nm corresponding to CP@H and CP@P samples, respectively, as calculated using the MDI Jade 5.0 software package. These results indicate that the craystal structures of CP@H and CP@P are similiar, but different. This may bring in some difference on the photocatalytic performance. The SEM images of CP@H and CP@P are shown in Fig. 2, in which the PhC_2Cu poly-

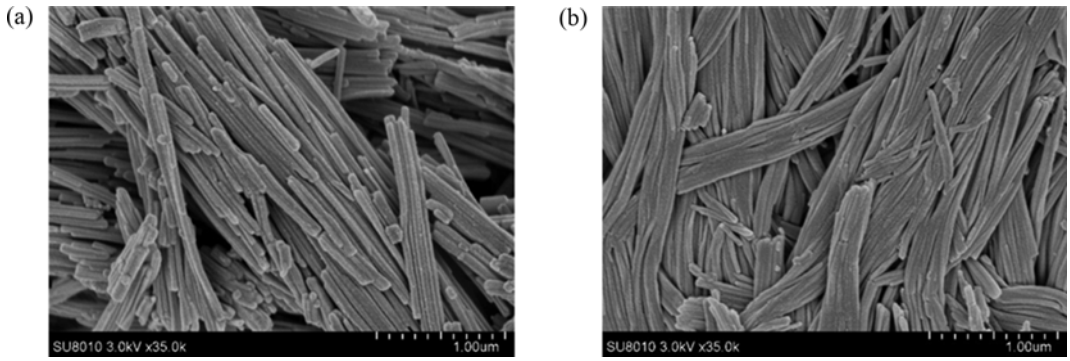

Fig. 2. SEM images of CP@H (a) and CP@P (b) solids.

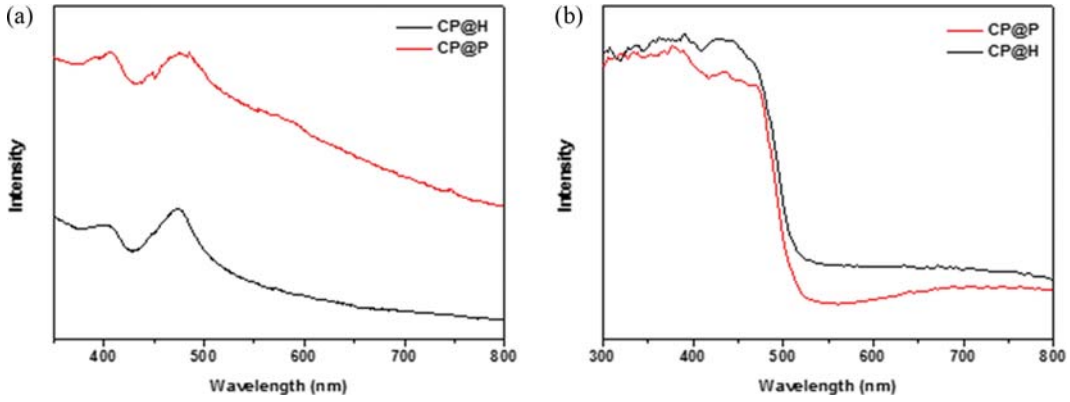

Fig. 3. (a) UV-vis absorbance spectra of CP@H and CP@P suspension in CH_3OH; (b) UV-vis absorption spectra of CP@H and CP@P solids.

mers are observed in both (a) and (b). Large amounts of nanobelts stick into bunches, and pile up. From the two images, we can see that the stacking ways of CP@H and CP@P are different; this would result in different crystal structures of the two samples.

The absorbance spectra of CP@H and CP@P suspensions and solids are displayed in Fig. 3, which are similiar to the previous report [21]. The suspensions in Fig. 3(a) show a wide range absorbance in the visible light region. According to the previous report, the peaks at about 405 nm are attributed to intraligand $\pi \rightarrow \pi^*$ transitions, while the peaks at about 475 nm are [d(Cu)$\rightarrow\pi^*$(C≡CPh)] metal-to-ligand chage transfer (MLCT) overlapping with the ligand-centered $\pi \rightarrow \pi^*$ transitions [27]. The absorption spectra of CP@H and CP@P solids are recorded by UV-vis diffuse reflectance spectroscopy and illustrated in Fig. 3(b), in which strong absorption from about 500 nm is observed. The visible-region absorption of CP@H and CP@P resulted from the intrinsic band gap of PhC_2Cu [21]. Differently, a wide absorption band in the range of 600-800 nm is also clearly observed in the spectra of CP@P, which is assigned to d-d transitions of Cu (II) [28,29], indicating the existence of Cu (II) in the sample of CP@P. This may be caused by the photoreduction of Cu (I) of PhC_2Cu [21]. The N_2 adsorption-desorption experiments give type III isotherms, indicating a typical isotherm of ordered organic-inorganic nanocomposites with hydrophobic surfaces [30]. Furthermore, it is also used to calculate the surface areas of CP@H and CP@P samples by Brunauer-Emmett-Teller (BET) theory, which are cooresponding to 26.66 cm^2/g and 10.96 cm^2/g, respectively.

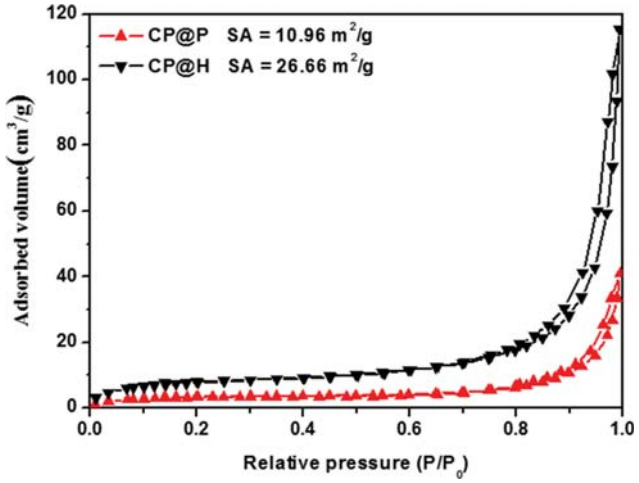

Fig. 4. N_2 adsorption-desorption isotherm of CP@H and CP@P.

The photocatalytic activity of as-prepared PhC_2Cu samples was evaluated by the degradation of MB aqueous solutions. MB is a typical pollutant for the ecological environment and human health, which can result in the generation decrease of Nicotinamide adenine dinucleotide (NADH) - dehydrogenase and the increase of the methemoglobin, further leading to nausea, bellyaches, headaches, dizziness, sweating, obnubilation, and so on. As illustrated

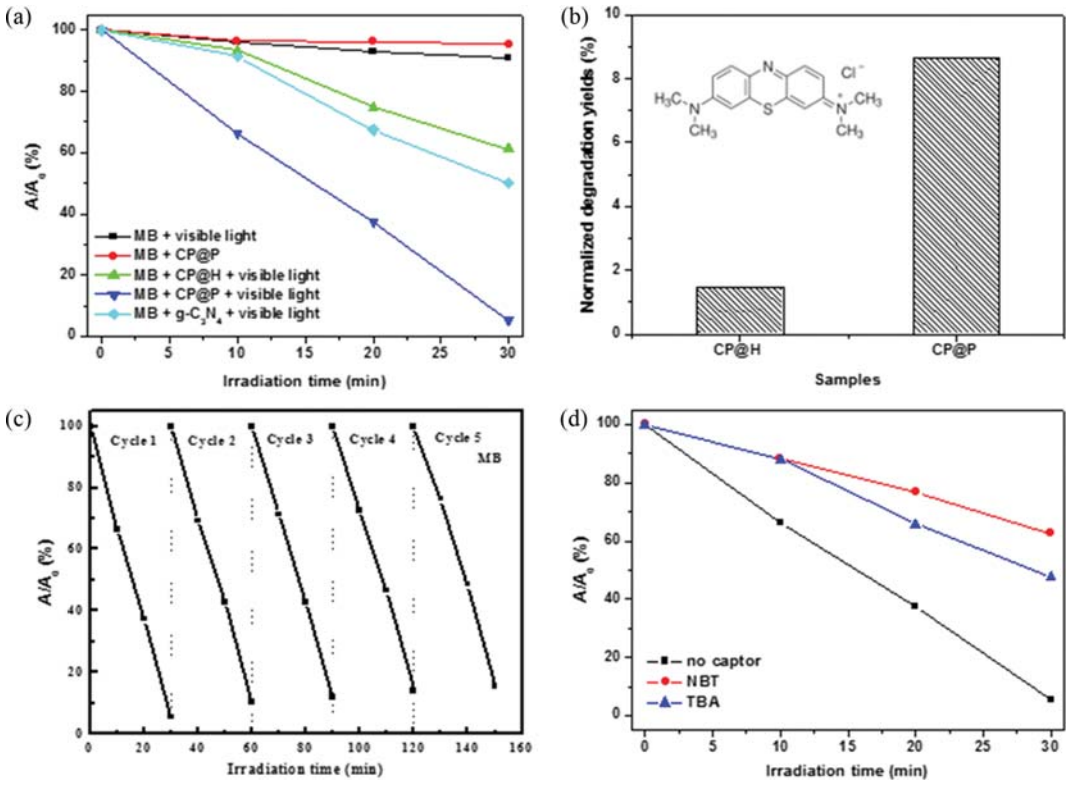

Fig. 5. (a) Photocatalytic degradation of MB by CP@H, CP@P and g-C_3N_4; (b) normalized degradation of MB by CP@H and CP@P for 30 minutes irradiation; (c) cyclic experiments for the photocatalytic degradation of MB by CP@P; (d) photocatalytic degradation of MB by CP@P in the presence of different captors.

in Fig. 5(a), both the CP@H and CP@P show significant degradation of MB under visible light irradiations, while negligible degradation is observed in the absence of either PhC_2Cu catalyst or visible light. We also compared the photocatalytic degradation of MB by PhC_2Cu samples to that by the previously reported high efficiency photocatalyst, g-C_3N_4. The results show that although the degradation rate of MB by g-C_3N_4 sample (~50% in 30 min) is a little faster than that by CP@H (~40% in 30 min), it is much slower than that by CP@P (~95% in 30 min). This shows the important roles of PhC_2Cu catalyst and visible light irradiations for the degradation of MB. From the figure, we can also see that the MB degradation by CP@P (~95%) is about 2.5-times higher than that by CP@H (~40%). To get a fair evaluation of the photocatalyst activity, the photocatalytic degradation of MB in 30 minutes is normalized in terms of the surface areas [31], as displayed in Fig. 5(b). It can be found that the normalized activity of CP@P is about six-times higher than that of CP@P. These results indicate that the photocatalytic activity of PhC_2Cu prepared by photo-synthesis method is much higher than that prepared by thermal-synthesis method. In addition, the stability of as-CP@P was also corroborated by the cyclic degradation of MB. The results in Fig. 5(c) show that CP@P remained active after five cycles, and the degradation rate of MB did not decrease obviously, suggesting a quite stable photocatalytic activity under present conditions.

As reported in the earlier research, the degradation of pollutants by PhC_2Cu mainly depends on the photocatalytic generation of reactive oxygen species (ROS), just like $O_2^{-\bullet}$ and •OH. Therefore, we degraded MB by CP@P in the presence of different captors upon visible light irradiation. As observed in Fig. 5(d), in the presence of NBT ($O_2^{-\bullet}$ captors) [24,25] and TBA (•OH) [31], the degradation of MB over CP@P significantly decresed. However, either NBT or TBA cannot absolutely inhibit the degradation of MB. These results mean that not only $O_2^{-\bullet}$ and •OH, but also the photogenerated conduction electrons can degrade MB. This process can be described by the following equations:

$$PhC_2Cu\ (I)+h\nu \rightarrow PhC_2Cu\ (II)+e^-_{CB} \quad (3)$$

$$e^-_{CB}+O_2 \rightarrow O_2^{-\bullet} \quad (4)$$

$$O_2^{-\bullet}+H^+ \rightarrow HO_2^{\bullet} \quad (5)$$

$$2HO_2^{\bullet} \rightarrow O_2+H_2O_2 \quad (6)$$

$$Cu\ (I)+H_2O_2 \rightarrow Cu\ (II)+\bullet OH+OH^- \quad (7)$$

$$H_2O_2+O_2^{-\bullet} \rightarrow \bullet OH+OH^-+O_2 \quad (8)$$

$$e^-_{CB}/O_2^{-\bullet}/\bullet OH+MB \rightarrow \text{inorganic smaller molecular} \quad (9)$$

To further prove the photocatalytic process we proposed based on the above results, the photogenerated $O_2^{-\bullet}$ and •OH in the visible light irradiated suspension of PhC_2Cu samples were also studied, respectively.

The generation of $O_2^{-\bullet}$ under photocatalytic conditions was quantified by its typical reaction with NBT [24,25]. Under visible light irradiation (Fig. 6), 17.6 μM $O_2^{-\bullet}$ was produced in 30 minutes by CP@P sample, which is 1.8-times higher than that produced by CP@H (9.65 μM). The generation of •OH was measured by its reaction with CA, generating CA-OH, which is a fluorescent product [26]. As displayed in Fig. 7, CA-OH adduct is generated over both CP@H and CP@P, suggesting the production of •OH. The production of CA-OH adduct by CP@P is apparently more than that by CP@H in the same irradiation time.

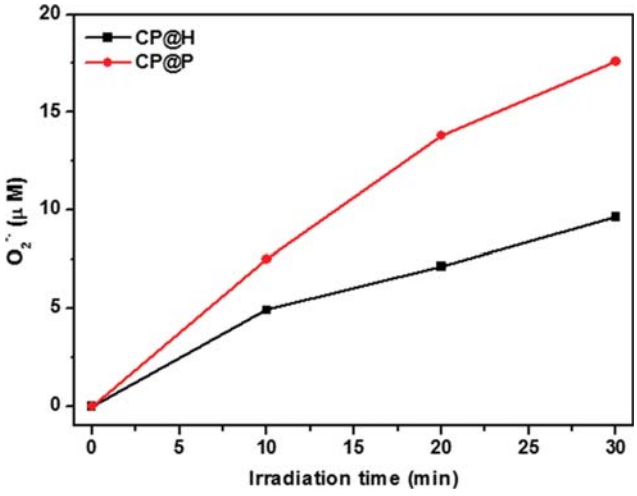

Fig. 6. Photocatalytic production of $O_2^{-\bullet}$ by CP@H and CP@P detedted by NBT method.

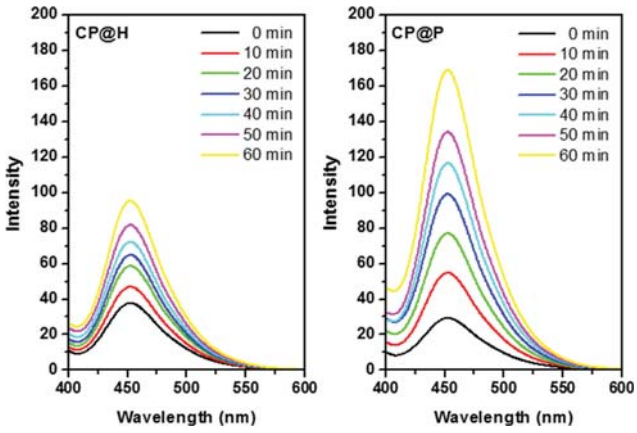

Fig. 7. Fluorescence emission intensity of coumarin-OH adduct (7-hydroxycoumarin) produced in the visible light irradiated suspension of CP@H and CP@P suspension.

Based on the results and analysis above, PhC_2Cu prepared by photosynthesis method shows much higher activity for the degradation of MB under visible light irradiation than that prepared by thermalsynthesis method. The higher photocatalytic activty of CP@P than CP@H may be attributed to more $O_2^{-\bullet}$ and •OH generation, which may intrisically result from the preferential exposure of photocatalytic active facet.

In summary, we synthesized PhC_2Cu nanobelt through two different methods, photo-synthesis and thermal-synthesis. According to the experimental results, the PhC_2Cu nanobelts prepared by photosynthesis method exhibit much higher photocatalytic activity than that prepared by traditional thermal-synthesis method for the degradation of MB. Meanwhile, the higher generation of $O_2^{-\bullet}$ and •OH by CP@P under visible light irradiation powerfully supports this conclusion. The higher photocatalytic activity is attributed to the

preferential exposure of photocatalytic active facet, which was charaterized by XRD spectra. In this work, photo-synthesis method is a safe and energy-saving method, because it happens at room temperature, while traditional thermal-synthesis method is dangerous due to the bumping problem. This study developed a new advanced method to prepare PhC_2Cu nanobelts with preferential active facet exposure, resulting in a higher photocatalytic activity under visible light irradiation.

ACKNOWLEDGEMENTS

The authors are grateful for the financial support of this work by National Natural Science Foundation of China (No. 21703170) and Top-rated Discipline construction scheme of Shaanxi higher education.

SUPPORTING INFORMATION

Additional information as noted in the text. This information is available via the Internet at http://www.springer.com/chemistry/journal/11814.

REFERENCES

1. C. Chen, W. Ma and J. Zhao, *Chem. Soc. Rev.*, **39**, 4206 (2010).
2. S. Ghosh, N. A. Kouamé, L. Ramos, S. Remita, A. Dazzi, A. Deniset-Besseau, P. Beaunier, F. Goubard, P.-H. Aubert and H. Remita, *Nat. Mater.*, **14**, 505 (2015).
3. J.-L. Wang, C. Wang and W. Lin, *ACS Catal.*, **2**, 2630 (2012).
4. C. Wang, Z. Xie, K. E. deKrafft and W. Lin, *J. Am. Chem. Soc.*, **133**, 13445 (2011).
5. J. Gao, J. Miao, P.-Z. Li, W. Y. Teng, L. Yang, Y. Zhao, B. Liu and Q. Zhang, *Chem. Commun.*, **50**, 3786 (2014).
6. Y. Fu, D. Sun, Y. Chen, R. Huang, Z. Ding, X. Fu and Z. Li, *Angew Chem. Int. Ed.*, **51**, 3364 (2012).
7. M. C. Das, H. Xu, Z. Wang, G. Srinivas, W. Zhou, Y.-F. Yue, V. N. Nesterov, G. Qian and B. Chen, *Chem. Commun.*, **47**, 11715 (2011).
8. T. R. Cook, Y.-R. Zheng and P. J. Stang, *Chem. Rev.*, **113**, 734 (2013).
9. E. M. Dias and C. Petit, *J. Mater. Chem. A*, **3**, 22484 (2015).
10. J. Y. Jing Li, Y.-Y. Liu and J.-F. Ma, *Chem. Eur. J.*, **21**, 4413 (2015).
11. B. Wu, W.-H. Zhang, Z.-G. Rena and J.-P. Lang, *Chem. Commun.*, **51**, 14893 (2015).
12. F. Wang, F.-L. Li, M.-M. Xu, H. Yu, J.-G. Zhang, H.-T. Xia and J.-P. Lang, *J. Mater. Chem. A*, **3**, 5908 (2015).
13. X.-L. Wang, J. Luan, F.-F. Sui, H.-Y. Lin, G.-C. Liu and C. Xu, *Cryst. Growth Des.*, **13**, 3561 (2013).
14. H. Zhang, G. Liu, L. Shi, H. Liu, T. Wang and J. Ye, *Nano Energy*, **22**, 149 (2016).
15. V. F. Plyusnin, A. V. Kolomeets, V. P. Grivin, S. V. Larionov and H. Lemmetyinen, *J. Phys. Chem. A*, **115**, 1763 (2011).
16. C. S. Smith and K. R. Mann, *J. Am. Chem. Soc.*, **134**, 8786 (2012).
17. T. Zhang and W. Lin, *Chem. Soc. Rev.*, **43**, 5982 (2014).
18. T. G. Moga, *Nat. Chem.*, **4**, 334 (2012).
19. G. Li, N. M. Dimitrijevic, L. Chen, T. Rajh and K. A. Gray, *J. Phys. Chem. C*, **112**, 19040 (2008).
20. M. Nishikawa, M. Fukuda, Y. Nakabayashi, N. Saito, N. Ogawa, T. Nakajima, K. Shinoda, T. Tsuchiya and Y. Nosaka, *Appl. Surf. Sci.*, **363**, 173 (2016).
21. H.-Y. Jiang, P. Zhou, Y. Wang, R. Duan, C. Chen, W. Song and J. Zhao, *Adv. Mater.*, **28**, 9776 (2016).
22. Y. Li, J. Xu, J. Chao, D. Chen, S. Ouyang, J. Ye and G. Shen, *J. Mater. Chem.*, **21**, 12852 (2011).
23. K. Cheng, W. Sun, H.-Y. Jiang, J. Liu and J. Lin, *J. Phys. Chem. C*, **117**, 14600 (2013).
24. H. Goto, Y. Hanada, T. Ohno and M. Matsumura, *J. Catal.*, **225**, 223 (2004).
25. Y. Yamakoshi, N. Umezawa, A. Ryu, K. Arakane, N. Miyata, Y. Goda, T. Masumizu and T. Nagano, *J. Am. Chem. Soc.*, **125**, 12803 (2003).
26. G. Liu, T. Wang, S. Ouyang, L. Liu, H. Jiang, Q. Yu, T. Kako and J. Ye, *J. Mater. Chem. A*, **3**, 8123 (2015).
27. S. S. Y. Chui, M. F. Y. Ng and C.-M. Che, *Chem. Eur. J.*, **11**, 1739 (2005).
28. J. Hu, H. Li, C. Huang, M. Liu and X. Qiu, *Appl. Catal. B: Environ.*, **142-143**, 598 (2013).
29. H.-Y. Jiang, G. Liu, M. Li, J. Liu, W. Sun, J. Ye and J. Lin, *Appl. Catal. B: Environ.*, **163**, 267 (2015).
30. M. Kruk and M. Jaroniec, *Chem. Mater.*, **13**, 3169 (2001).
31. H.-Y, Jiang, J. Liu, K. Cheng, W. Sun and J. Lin, *J. Phys, Chem. C*, **117**, 20029 (2013).

Supporting Information

Photo-synthesized copper phenylacetylide nanobelts with preferential photocatalytic active facet exposure

Xinglong Xie[‡], Yu Qiu[‡], Sen Zhao, Hai-Ying Jiang[†], and Jinjun Lu

Key Lab of Synthetic and Natural Functional Molecule Chemistry of Ministry of Education, College of Chemistry & Materials Science, Northwest University, Xi'an 710127, P. R. China
(*Received 29 March 2018 • accepted 18 July 2018*)

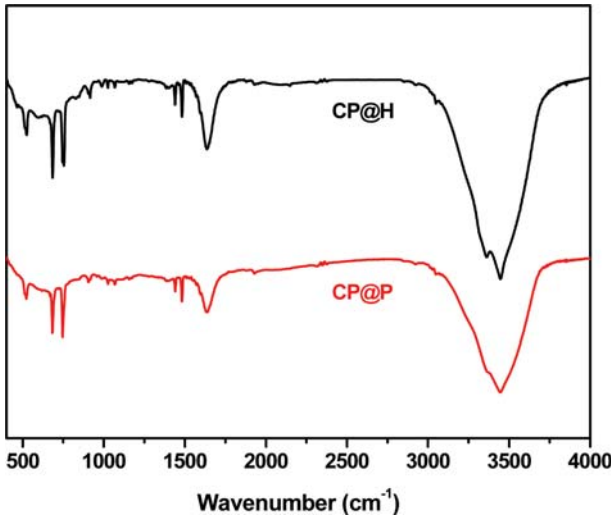

Fig. S1. FT-IR spectra of CP@H and CP@P solids [1,2]: The peak at 513 cm^{-1} is attributed to the vibration of C-C≡C bond; the peaks at 525 cm^{-1}, 685 cm^{-1}, 1,441 cm^{-1} and 1,483 cm^{-1} are assigned to the vibrations of C-C bonds; the peaks at 746 cm^{-1}, 847 cm^{-1}, 916 cm^{-1} and 988 cm^{-1} are derived from the vibrations of C-H bonds; the peaks at 1,632 cm^{-1}, 1,639 cm^{-1}, 3,362 cm^{-1} and 3,446 cm^{-1} are ascribed to the vibrations of adsorbed H_2O molecular on the surface.

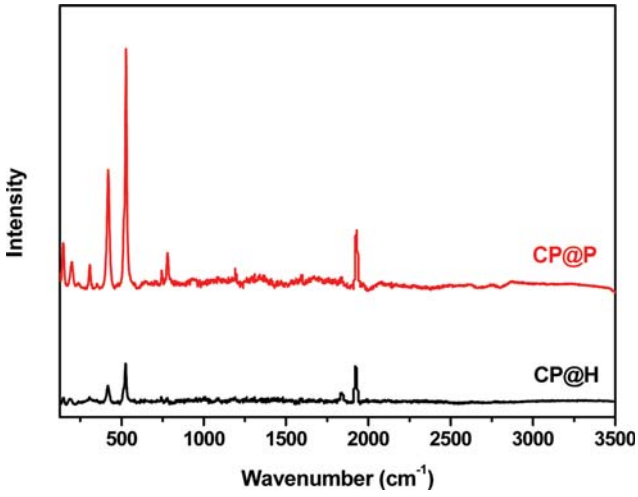

Fig. S2. Raman spectra of CP@H and CP@P solids [1,2]: The peaks at 1,971 cm^{-1}, 1,928 cm^{-1}, 1,839 cm^{-1}, 308 cm^{-1}, 200 cm^{-1}, and 144 cm^{-1} are attributed to the vibration of the triple bonds of sp C; the peaks at 746 cm^{-1} are ascribed to the vibration of C-H bonds; the peaks at 1,595 cm^{-1}, 781 cm^{-1}, 623 cm^{-1} and 422 cm^{-1} belong to the C-C single bonds; the peaks at 529 cm^{-1}, 1,000 cm^{-1} and 1,595 cm^{-1} are derived from the vibration of C-Cu bond, ring breathing, and E2g mode for in-phase stretch of sp^2 C, respectively.

1. I. A. Garewsova, V. T. Alexanjan, L. A. Leites, I. A. Leites, I. R. Golding and A. M. Sladkov, *J. Organomet. Chem.*, **13**, 3169 (1973).
2. Stephen S. Y. Chui, Miro F. Y. Ng and Chi-Ming Che, *Chem. Eur. J.*, **11**, 1739 (2005).